Catalytic oxidation of formaldehyde on surface of H—TiO2/H—C—TiO2 without light illumination at room temperature

Lei Zeng [a], Wulin Song [a,b,*], Minghui Li [a], Dawen Zeng [a], Changsheng Xie [a]

[a] *State Key Lab of Materials Processing and Die & Mould Technology, Huazhong University of Science and Technology, Wuhan 430074, PR China*
[b] *Analytic and Testing Center, Huazhong University of Science and Technology, Wuhan 430074, PR China*

ABSTRACT

A modified TiO$_2$ was prepared by short-time annealing in low concentration of hydrogen gas at low temperature and ordinary pressure. As a result, the hydrogenated TiO$_2$ (H—TiO$_2$) and hydrogenated carbon-doped TiO$_2$ (H—C—TiO$_2$) could decompose gaseous formaldehyde without light irradiation at room temperature. Compared with pure TiO$_2$, the H—TiO$_2$ and H—C—TiO$_2$ were allowed to introduce more oxygen vacancies and surface hydroxyl groups, which had crucial contribution to catalytic oxidation of gaseous formaldehyde in the dark. Moreover, the existence of oxygen vacancies and surface hydroxyl groups were confirmed by XPS and EPR. Oxygen vacancies could efficiently govern O$_2$ adsorption by trapping O$_2$ molecules on defect sites and producing active oxygen species. The surface hydroxyl groups could facilitate the adsorption of O$_2$ molecules and remove carbonate species which could block the catalytic active sites. Based on these results, a novel mechanism of gaseous formaldehyde decomposed by hydrogenated TiO$_2$ in the dark was proposed.

© 2013 Elsevier B.V. All rights reserved.

1. Introduction

It is generally known that formaldehyde does great harm to people's health. Hence, it is necessary to remove indoor formaldehyde, and heterogeneous catalysis is one of the most effective solutions.

In 1972, the group of Fujishima and Honda discovered the phenomena of photocatalytic splitting of water on TiO$_2$ electrode under ultraviolet light [1–3]. Since then, enormous efforts have been devoted to the research of TiO$_2$ material, which has led to many promising applications ranging from photovoltaics and photocatalysis to photochromics and sensors [4–7]. With the rise of people's demand on inhabitancy environment, more and more people are realizing the importance of the indoor air quality. Within this respect, photocatalytic degradation of volatile organic compounds (VOCs) is one of the most promising methods. TiO$_2$ as the typical photocatalyst has been widely investigated, and various methods have been developed to make TiO$_2$ decompose VOCs under visible light illumination, such as doping, sensitization, coupling with narrow band gap semiconductor and loading noble metal or quantum dots [8–14]. Xu et al. [15] have reported that cerium doped titania photocatalytically degrades an aqueous

suspension of formaldehyde under visible light and the mechanism of the photocatalytic activity enhancement has also been investigated. Photocatalytic oxidation of formaldehyde by C, N, S-tridoped titania powders under sunlight has also been reported, and the high photocatalytic activity is attributed to the results of the synergetic effects between C, N and S [16]. Akbarzadeh et al. [17] have reported that formaldehyde and methylene blue solution could be well removed by vanadia–titania thin films under sunlight and have also discussed the optimum ratio between vanadia and titania. Despite their best efforts, formaldehyde could be decomposed only under visible light illumination. Nevertheless, the degradation of formaldehyde in the dark has been rarely reported, previously.

In recent years, thermocatalysis has successfully attracted the interest of researchers. Álvarez et al. [18] have reported that complete conversion of formaldehyde was achieved over a Pd/Al$_2$O$_3$ catalyst at 90 °C. Moreover, complete conversion of formaldehyde by TiO$_2$ supported Pd nanoparticles at room temperature has been investigated [19]. The effects of different supported materials on catalytic oxidation of formaldehyde at low temperatures have been compared, and 0.6 wt.% Pt/TiO$_2$ is the most active as the reason for decomposing formaldehyde is ascribed to the strong metal-support interaction [20]. Even like this, the cost of noble metal still presents an obstacle for the commercialization of this catalyst. Thus, it is necessary to design a catalyst which is facile to prepare in quantity and decompose organic pollutant in an economical and efficient way.

* Corresponding author at: State Key Lab of Materials Processing and Die & Mould Technology, Huazhong University of Science and Technology, Wuhan 430074, PR China. Tel.: +86 27 87557453; fax: +86 27 87557453.
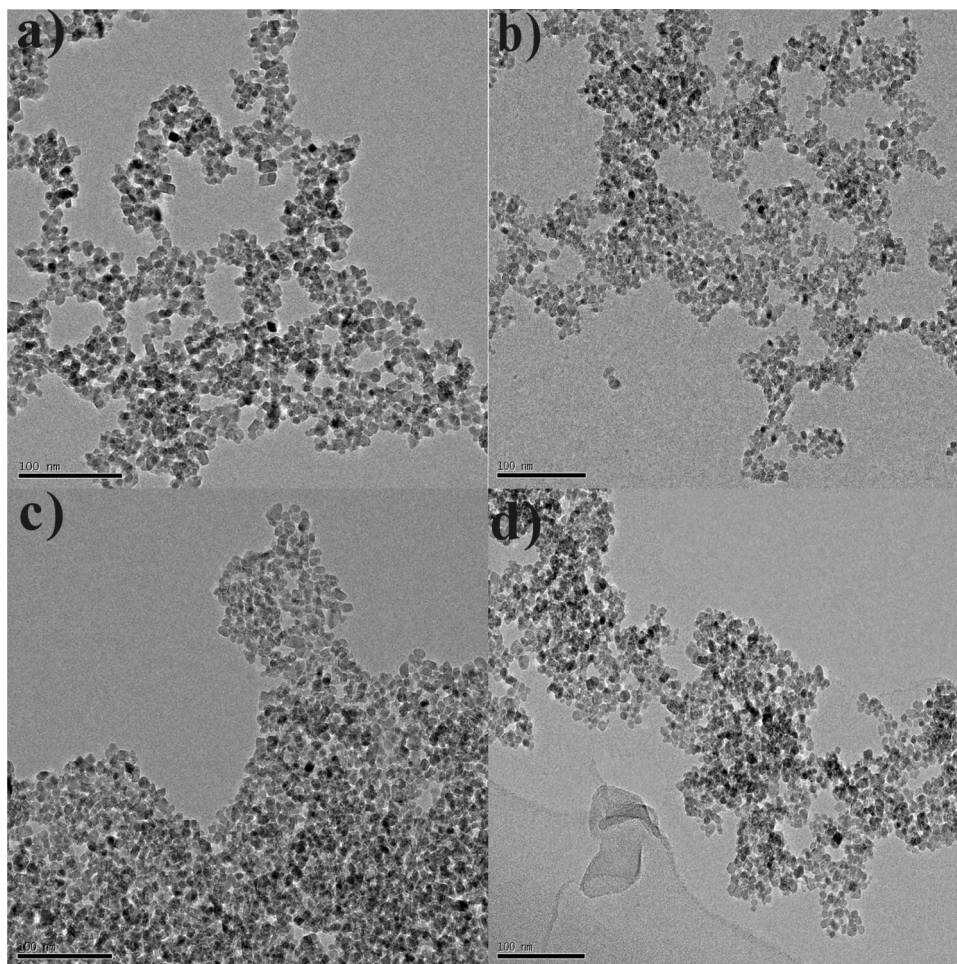*E-mail address:* wulins@126.com (W. Song).

Fig. 1. TEM image of pure TiO_2 (a), C—TiO_2 (b), H—TiO_2 (c), H—C—TiO_2 (d).

The work of Chen et al. [21] inspired us to undertake our present research. They engineered a black highly efficient photocatalytically active TiO_2 which could even respond to infrared light by hydrogenation treatment under high pressure (20.0-bar H_2 atmosphere) at 200 °C for 5 days, and they attributed the enhancement of photocatalysis activity to surface disordered layer. However, the processing condition including the high pressure apparatus, long processing time, and high concentration of hydrogen restricted its spread. In this work, a modified TiO_2 was prepared by a simple and economical method (annealing in low concentration of hydrogen atmosphere at low temperature and ordinary pressure). Surprisingly, the concentration of the formaldehyde is decomposed about 53%, 57% for H—TiO_2 and H—C—TiO_2 without light irradiation at room temperature during 4 h reaction, respectively. However, C-doped TiO_2 as the most active photocatalyst unexpectedly showed a worse performance than the hydrogenated samples under the same experiment condition. Furthermore, the synergistic effects between oxygen vacancies and C dopants were not obvious. The catalysts were characterized by X-ray diffraction (XRD), BET surface areas, X-ray photoelectron spectroscopy (XPS), transmission electron microscopy (TEM), electron paramagnetic resonance (EPR), and Raman spectra. A simplified mechanism, different from the conventional photocatalytic mechanism, is proposed to explain the high catalytic activity of TiO_2. Our findings might have the potential to expand the application of TiO_2 to the other fields, such as degradation of indoor VOCs in the dark or in submarines or other low-light environments.

2. Experiment

2.1. Material preparation

All chemicals were purchased and used without further purification including tetrabutyl titanate (TTIP, 98%; Sinopharm Chemical Reagent Co., Ltd.), ethylene glycol (EG; Sinopharm Chemical Reagent Co., Ltd.), gas mixture of H_2 and Ar (5% H_2 in Ar).

2.1.1. Hydrothermal synthesis

At first, 1 mL TTIP was dissolved in 25 mL EG at room temperature. Then, the above solution was added dropwise to the 50 mL deionized water under vigorous stirring for 30 min. Suspension solution was obtained after stirring and transferred into a 100 mL Teflon-lined autoclave. The autoclave was sealed and maintained at 180 °C for 10 h. After the hydrothermal reaction completed, the resulting product was centrifuged and rinsed with ethanol and water for several times to remove residual EG on the surface. The obtained pale yellow precipitate was dried at 80 °C in a vacuum oven. The final C-doped TiO_2 was prepared and the pure TiO_2 was obtained under the same condition only in the absence of EG.

2.1.2. Thermal treatments

The pure TiO_2 and C-doped TiO_2 were placed into a tube furnace, then the tube was filled with desired gases (H_2/Ar). The current velocity of H_2/Ar (20 mL/min) was controlled by gas flow controller during annealing. The exhaust line was bubbled through a cup
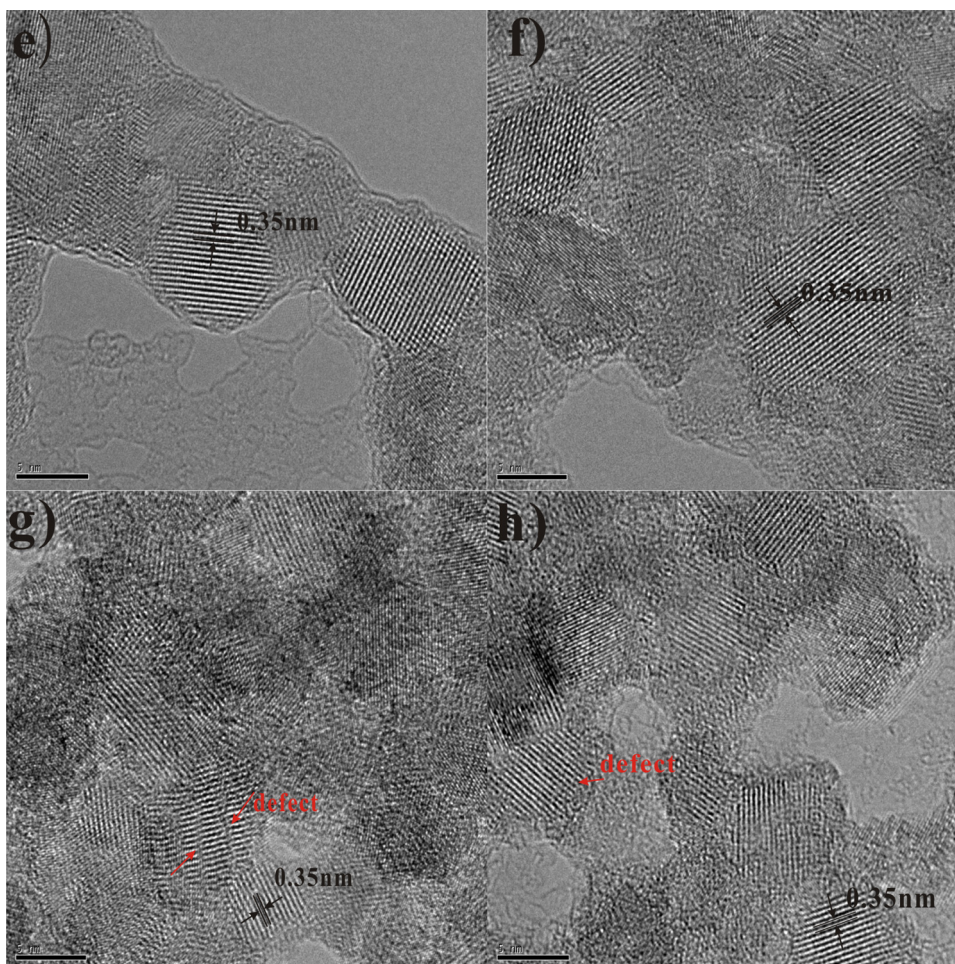
Fig. 2. HRTEM image of pure TiO_2 (e), C—TiO_2 (f), H—TiO_2 (g), H—C—TiO_2 (h).

of water (the exhaust line was kept ∼5 cm below the water surface). The hydrogen-treated samples were prepared by annealing in H_2/Ar at 300 °C for 2 h (the heating rate was 5 °C/min), and labeled as H—TiO_2 and H—C—TiO_2, respectively.

2.2. Material characterization

The morphologies of samples were observed by high-resolution transmission electron microscopy (HRTEM, FEI Tecnai G^2 F30 field-emission TEM). X-ray diffraction (XRD) patterns were collected with X'Pert PRO diffractometer (PANalytical B.V., Almelo, the Netherlands, CuK_α radiation with λ=1.5406 Å) in 2θ range from 10° to 90°. EPR spectra were registered at 293 K using a Bruker 220 SE spectrometer, at a microwave frequency of 9.8 GHz. The Raman spectra were gained by using a LabRAM HR spectrometer (HORIBA Jobin Yvon, France) with a laser excitation of 532 nm. X-ray photoelectron spectroscopy (XPS) measurements were performed in a VG Multilab2000 spectrometer to obtain information on the chemical binding energy of the samples. The specific surface areas (SSA) of the powders were determined in a Flow Sorb ASAP 2020 apparatus (Micromeritics) by using the single-point BET method.

3. Catalytic activity test

Catalytic degradation was tested in the self-designed reactor. The whole system is composed of reacting chamber, cushion chamber and gas concentration detector (Photoacoustic IR Multi-gas Monitor (model 1412; INNOVA Air Tech Instruments)). The detector could detect ppm-level of formaldehyde, water vapor and carbon dioxide in our experiment. In this paper, formaldehyde was chosen as a model pollutant. Firstly, 100 mg pure TiO_2 powders were put into reacting chamber. Soon afterwards formaldehyde solution was injected into the reactor and volatilized until they reached absorption/desorption equilibrium. The initial concentration of formaldehyde was 100 ppm ($\pm$5 ppm). The experiment was conducted at ambient temperature and the catalytic activity test lasted for 4 h. After testing the catalytic activity of pure TiO_2, then the samples C—TiO_2, H—TiO_2 and H—C—TiO_2 was tested under the same condition in turn.

4. Results and discussion

4.1. TEM characterization

Fig. 1 shows the typical TEM images of selected samples. The particle sizes can be directly compared since each image is shown with the same scale bar. These images show that nanoparticles tend to aggregate. Analysis of Fig. 1 showed that the distribution of particle size is uniform, and the particle size is around 15 nm, 12 nm, 18 nm, 13 nm, respectively. As the HRTEM images shown in Fig. 2, it is evident to see that such grains are comprised of highly crystallized anatase with lattice of 0.35 nm which is corresponding to the (1 0 1) crystallographic plane of TiO_2. The lattice fringes of pure TiO_2 and
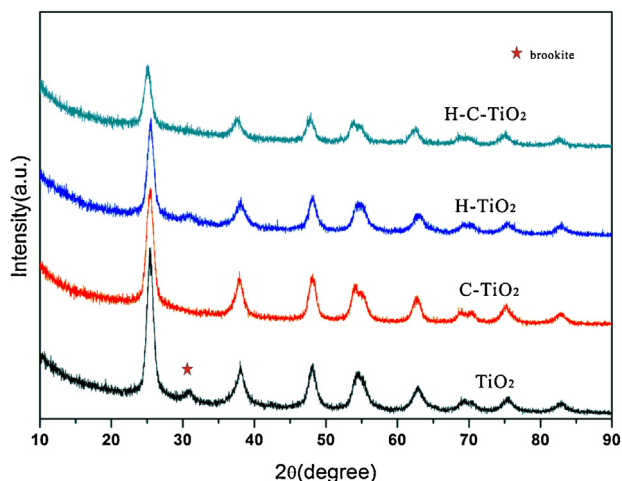
Fig. 3. XRD patterns of TiO₂, C—TiO₂, H—TiO₂, H—C—TiO₂.

Fig. 4. Raman spectra of pure TiO₂, C—TiO₂, H—TiO₂ and H—C—TiO₂.

C—TiO₂ are distinct, while fuzzy in hydrogenated samples, which is consistent with Zhang's report [22]. From the HRTEM images, it can be also observed that lattice defects exited in hydrogenated samples (which are indicated by red arrows in picture (g) and (h) of Fig. 2), and it confirms that lattice defects have been introduced in hydrogenation process and the microstructure of TiO₂ have been changed.

4.2. XRD characterization

The XRD measurement is carried out to investigate the phase and structure of synthesized samples. As shown in Fig. 3, the XRD patterns of the pure TiO₂ can be indexed to anatase (JCPDS file No. 21-1272) and brookite (JCPDS file No. 03-0380). The existence of brookite may be related to the low hydrothermal temperature. However, the peak around 30° which is mainly indexed to brookite is weakened in H—TiO₂, while it disappears in C—TiO₂ and H—C—TiO₂. This may be related to the different processing condition. Hydrogenation as a clean processing procedure can retard the phase transformation happen [23]. The average crystalline sizes of TiO₂, C—TiO₂, H—TiO₂, and H—C—TiO₂ are estimated as 14.2 nm, 11.7 nm, 15.5 nm, and 12.8 nm by using Scherer formula, respectively. The calculated values are in good agreement with the observed particle sizes from the TEM images. Analyzing the variation of crystalline sizes, it is suggested that the growth of crystal is inhibited after doping but promoted after annealing in hydrogen gas. The main peak of H—C—TiO₂ shifting to lower value is also observed, which suggests that C element may have been incorporated into the lattice of TiO₂ successfully.

4.3. Raman spectra

Structure properties of all samples were further examined by measuring Raman scattering. As shown in Fig. 4, the Raman active modes locate at ~144 cm^{-1} (E_g), 197 cm^{-1} (E_g), 400 cm^{-1} (B_{1g}), 519 cm^{-1} (B_{1g}), and 639 cm^{-1} (E_g) are detected for all samples, indicating that all samples are mainly composed of anatase phase. However, the Raman intensity of main E_g mode has weakened after C doping. It may be ascribed to the fact that C atom has been incorporated into the lattice of TiO₂ and the formation of Ti—O—C band leads to the decreasing of Raman activity. As shown in the inset of Fig. 4, the main E_g mode of modified samples broadens and shifts toward high wavenumbers with respect to that of pure TiO₂. As is well known, the blue-shift and broadening of lowest frequency E_g mode of TiO₂ are the results of the finite size of grain size (<10 nm) or shortening of correlation length for the presence of defects
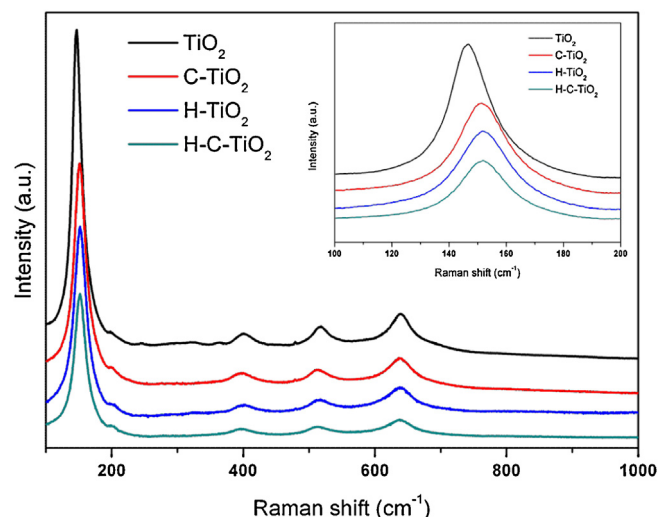
[24,25]. However, the size of crystallites obtained from our XRD data ($D > 10$ nm for all samples) exclude the occurrence of finite-size effects. Consequently, the presence of defects is rather responsible for the blue-shift and broadening of E_g peak of the modified TiO₂. For both of C doped and hydrogenated TiO₂, the possible defects are only oxygen vacancies (Ti^{3+} sites) [26]. Since C atom inserting the TiO₂ host matrix should form oxygen vacancies to balance charge around dopants. Hydrogenation is a clean process which did not introduce impurities except point defects (oxygen vacancies) into the TiO₂ structure. Similar results have also been reported by other groups. For example, Jiang et al. [27] characterized oxygen vacancy associates within hydrogenated TiO₂ by positron annihilation lifetime spectroscopy. Lu et al. [28] also reported that oxygen vacancy formed in TiO₂ nanotube arrays through annealing in hydrogen atmosphere.

4.4. EPR measurement

To confirm the formation of defect sites in catalyst, EPR analysis was used to characterize the all samples. Fig. 5 displays the EPR spectra measured at 293 K of all samples without light illumination. From inset of Fig. 5, no EPR signal is detected for pure TiO₂, it
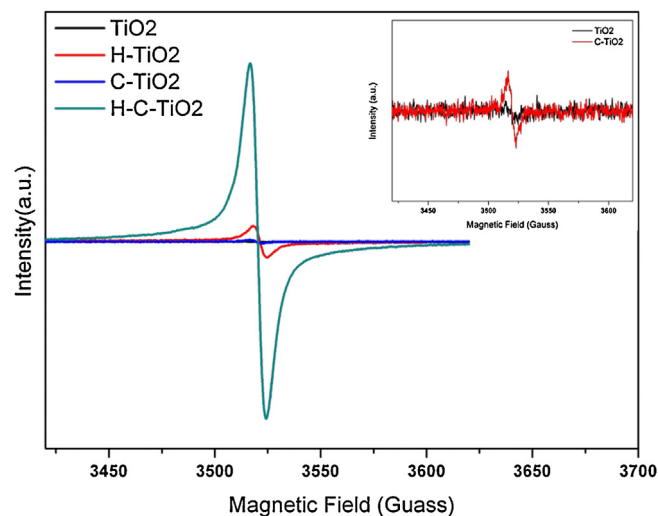

Fig. 5. EPR spectra recorded at 293 K for TiO₂, H—TiO₂, C—TiO₂ and H—C—TiO₂ samples.
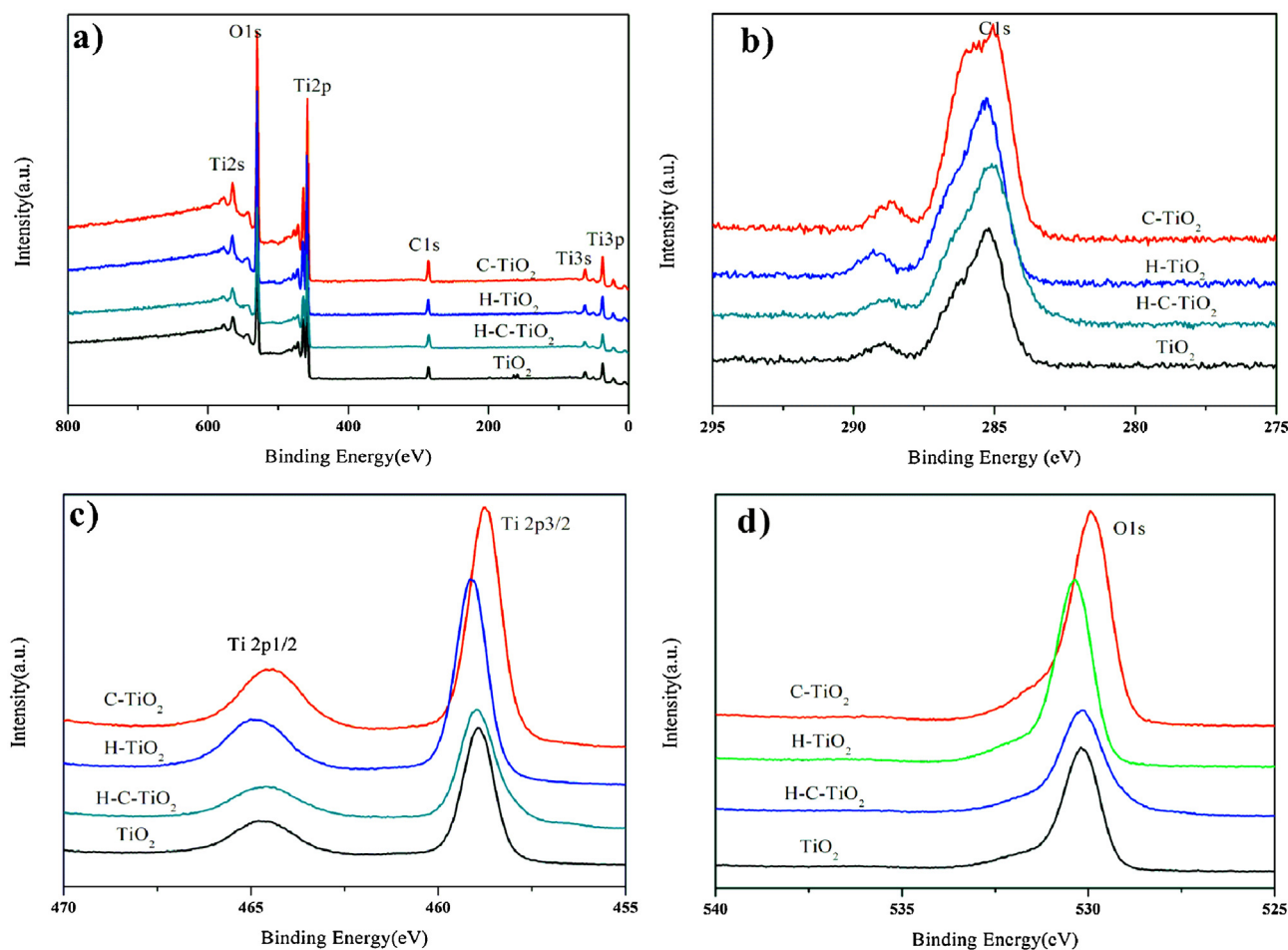
Fig. 6. XPS spectra (a) survey spectrum, (b) C1s, (c) O1s and (d) Ti2p for different samples.

suggests that free of paramagnetic species exist in pure TiO$_2$. For the C–TiO$_2$ sample, a signal at $g = 2.004$ is yielded in EPR spectra. Similar patterns for signal at $g = 2.004$ in anion doped TiO$_2$ have been reported in literature [29] and attributed to defects (like oxygen vacancy with one electron). When the samples are reduced by hydrogen gas at 300 °C, an apparent symmetrical and sharp signal at $g = 2.003$ appears in both H–TiO$_2$ and H–C–TiO$_2$. It is assigned to the presence of an electron trapped on an oxygen vacancy in the bulk [30], which confirms the observation of HRTEM. The signal at $g < 2$ is attributed to Ti^{3+} species is not yielded in the hydrogenated TiO$_2$. This may be related to testing environment, the Ti^{3+} species can be detected by EPR measurement at 77 K [31]. From the EPR spectra, it is also observed that the intensity of the feature at $g = 2.003$ for the H–C–TiO$_2$ is much stronger than the feature for H–TiO$_2$, which indicates that the concentration of oxygen vacancies for H–C–TiO$_2$ is higher than H–TiO$_2$.

4.5. XPS spectra

The surface chemical composition and chemical states of all samples were characterized by XPS, as shown in Fig. 6. All samples contain Ti, O and C elements, and the core level peak of each element has shifted after modifying, it means that chemical states have been changed. Fig. 7 shows C 1s spectra for all samples. For pure TiO$_2$, three kinds of surface carbon species are observed in the C 1s spectra. The first peak at 284.8 eV is usually assigned to adventitious carbon contamination absorbed from the ambient, which cannot be eliminated. The second peak locates at

around 285–286.5 eV is ascribed to element carbon [32]. After carbon doping, the intensity of second peak increases, it suggests that large amounts of carbon exist on its surface. The third peak for TiO$_2$ and H–TiO$_2$ locates at 288.9 eV, which is ascribed to carbonate species adsorbed on the surface of TiO$_2$ and H–TiO$_2$ samples, respectively. For C–TiO$_2$ and H–C–TiO$_2$, the BE peaks center at 288.6 eV indicates that C–O bond has formed, which means that the carbon atom may be incorporated into interstitial positions of the TiO$_2$ lattice [33–36]. Interestingly, the binding energy of C 1s of carbon species is not altered after H$_2$ reduction. This indicates that the chemical nature of carbon species in C–TiO$_2$ is not influenced by H$_2$ reduction treatment.

The values of Ti 2p$_{1/2}$ and Ti 2p$_{3/2}$, and the difference between the Ti 2p$_{1/2}$ and Ti 2p$_{3/2}$ for all samples were added in Table 1. For pure TiO$_2$ samples, the XPS spectra have a split of 5.7 eV between the Ti 2p$_{1/2}$ and Ti 2p$_{3/2}$, which indicates that Ti exists in the form of

Table 1
Surface O/Ti ratios for all samples from XPS spectra.

Sample	TiO$_2$	C–TiO$_2$	H–TiO$_2$	H–C–TiO$_2$
Ti 2p3/2 (eV)	458.93	458.75	459.14	458.90
Ti 2p1/2 (eV)	464.64	464.43	464.81	464.54
$\triangle$(Ti 2p1/2 – Ti 2p3/2) (eV)	5.71	5.68	5.67	5.64
O$_L$/Ti	2.10	2.04	1.95	2.00
O$_C$/Ti	0.51	0.11	0.68	0.53
O$_H$/Ti	0.21	0.14	0.21	0.22

O$_L$: O 1s core level peak at ca. 529.9 eV for TiO$_2$.
O$_C$: O 1s core level peak at ca. 530.4 eV for TiO$_2$.
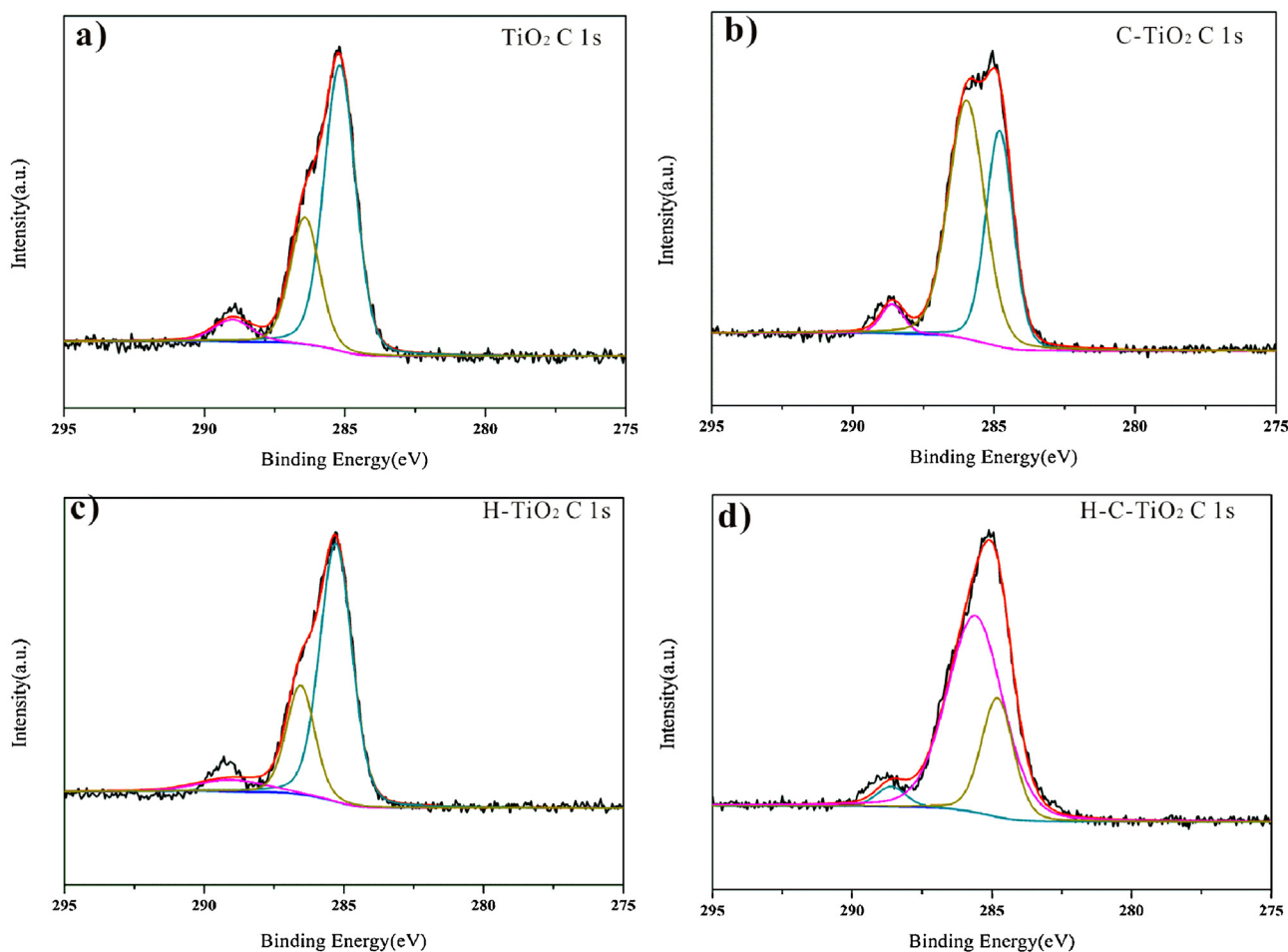O$_H$: O 1s core level peak at ca. 531.6 eV for TiO$_2$.

Fig. 7. C 1s XPS spectra for TiO_2, $C-TiO_2$, $H-TiO_2$, $H-C-TiO_2$.

Ti^{4+} [37]. On account of instability of Ti^{3+}, for all modified samples, no peaks related to Ti^{3+} are detected. This observation demonstrates that the surfaces of these three samples are dominated by Ti^{4+}. However, the binding energy difference between the doublets decreases after doing and H_2 reduction, also indicating the formation of oxygen vacancies in modified samples, and it corresponds with the results of EPR measurements. Furthermore, there is a negative shift of Ti 2p peaks after doping, it can be also suggested that the carbon atoms have been indeed incorporated into the interstitial positions of TiO_2 lattice, which is in good accordance with previous reports [38–40].

Fig. 8 shows O 1s XPS spectra for all samples. For pure TiO2, three kinds of surface oxygen species are observed. A main peak belonging to the lattice oxygen atoms occurs at ca. 529.9 eV (labeled as O_L), surface hydroxyl group at ca. 531.6 eV (labeled as O_H), and chemisorbed O_2 at around ca. 530.4 eV (labeled as O_C), respectively. O/Ti ratios on catalyst surface estimated from XPS spectra are given in Table 1. After C doped ($C-TiO_2$ sample), O_L/Ti ratio, O_H/Ti ratio and O_C/Ti ratio decrease, indicating that hydroxyl groups are substituted by carbon atoms and defect sites are generated on TiO_2 surface. After H_2 reduction of $C-TiO_2$ at 300 °C ($H-C-TiO_2$ sample), O_H/Ti ratio is recovery and O_C/Ti ratio is further enhanced. This implies that defect sites and hydroxyl groups are formed simultaneously, which is consistent with the observation in pure TiO_2 system with H_2 reduction treatment. Especially, the O_C/Ti ratio increases apparently, indicating that $H-TiO_2$ prefer to adsorb O_2, which is consistent with literature [41].

4.6. Catalyst activity

Fig. 9 displays the catalytic properties of four samples. Catalytic oxidation of formaldehyde by TiO_2 and $C-TiO_2$ are negligible, indicating that these two samples have no catalytic activity in the dark. However, the hydrogenated samples demonstrate high catalytic activity in the same testing condition. The concentration of the formaldehyde is decomposed about 53%, 57% for $H-TiO_2$ and $H-C-TiO_2$ during 4 h reaction, respectively. To confirm the result, the specific surface area of TiO_2, $C-TiO_2$, $H-TiO_2$, and $H-C-TiO_2$ are calculated using Brunauer-Emmett-Teller (BET) equation, and the result are 168.3 m^2/g, 186.0 m^2/g, 136.6 m^2/g, 159.9 m^2/g, respectively. Analysis of the BET results, the specific surface areas of samples have been decreased apparently after annealing in hydrogen gas. Therefore, we are pretty sure that the decreased concentration of formaldehyde is not induced by adsorption. It is postulated that the oxygen vacancies induced by hydrogenation are responsible for the catalytic activities of these catalyst in the dark.

4.7. Mechanism discussion

Based on above results, the microstructure of all samples varied with different processing treatment is schematically exhibited in Fig. 10. Upon the incorporation of carbon into TiO_2 ($C-TiO_2$), defect sites have been introduced into the obtained samples, the catalytic activity is still negligible. This may be ascribed to that the
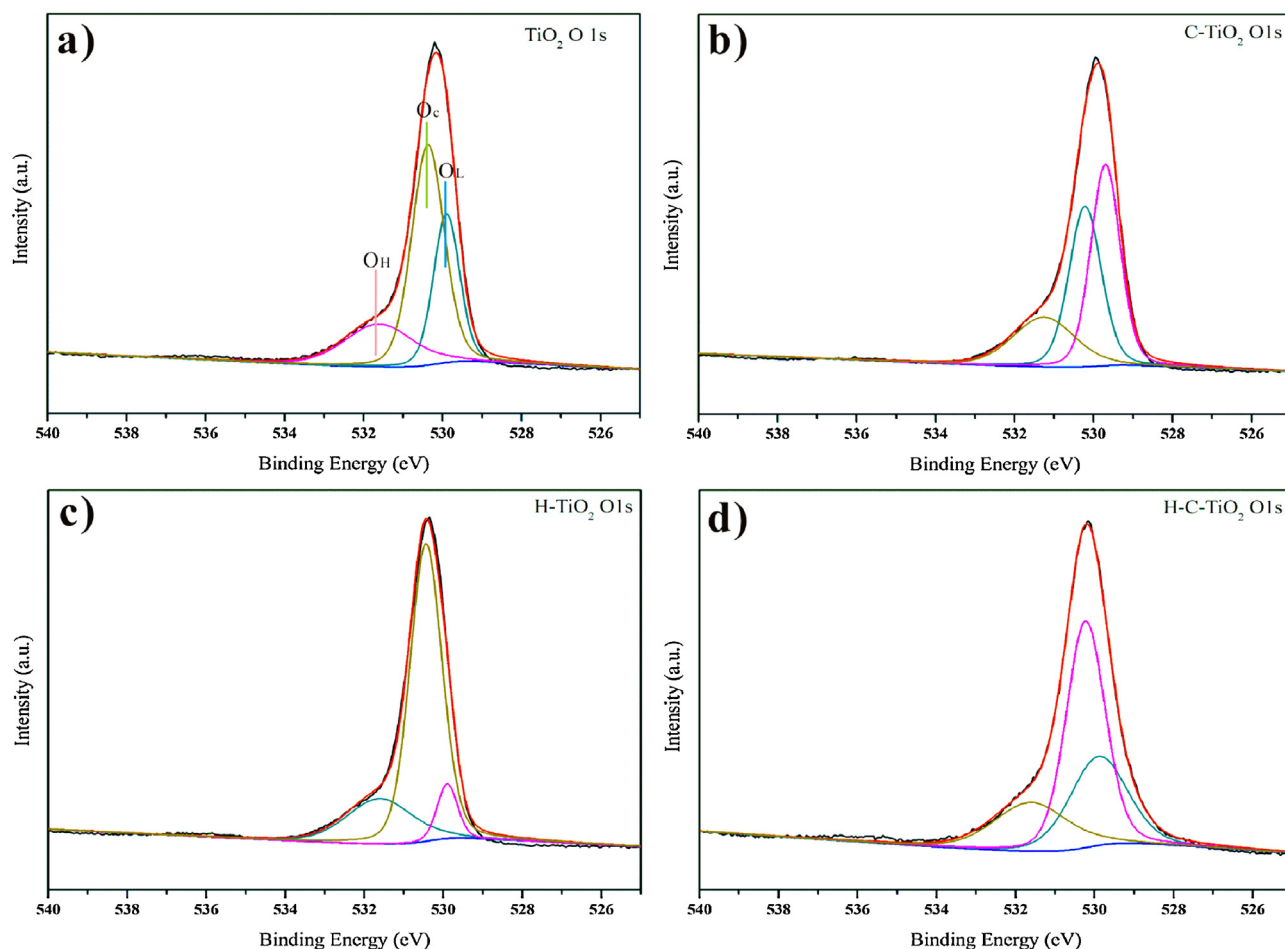
Fig. 8. O 1s XPS spectra for TiO_2, C—TiO_2, H—TiO_2, H—C—TiO_2.

amount of hydroxyl group and chemisorbed O_2 have decreased while the amount of surface carbonate species have increased, and the defects induced by doping cannot transform oxygen molecules to active oxygen species. Consequently, it is difficult to degrade HCHO into CO_2 in dark environment. After reduction of TiO_2 (H—TiO_2), large quantity of oxygen vacancies and chemisorbed O_2 are generated. The oxygen vacancies are favorable to reduce the chemical adsorption energy of oxygen molecule adsorbing on the surface of TiO_2. Moreover, chemisorbed O_2 accept electrons from

oxygen vacancies, then, be transformed into active oxygen species [41–45]. As we know, the surface hydroxyl group is beneficial to remove carbonate species to avoid blocking active sites. Thus, when H—TiO_2 samples are exposed to formaldehyde atmosphere, the HCHO molecules are adsorbed on surface hydroxyl group rapidly, oxygen molecules are also adsorbed on surface sites which are closed to defect sites and be transformed to active oxygen species. Then HCHO molecules are oxidized into formate surface species by reacting with active oxygen species, and formate are directly
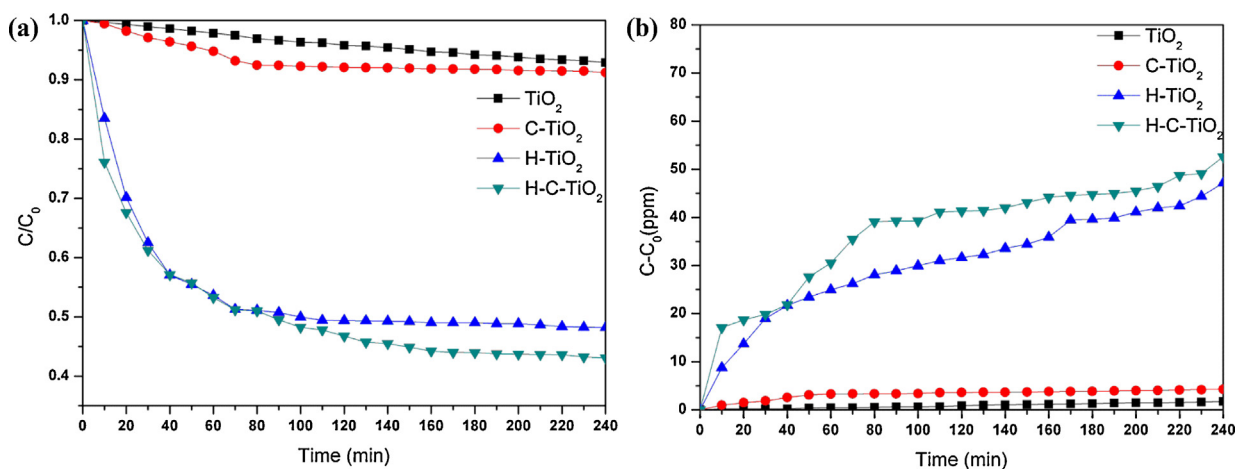

Fig. 9. Catalytic decomposition of formaldehyde (a) and CO_2 generation (b) using TiO_2, C—TiO_2, H—TiO_2 and H—C—TiO_2 without light irradiation at room temperature.
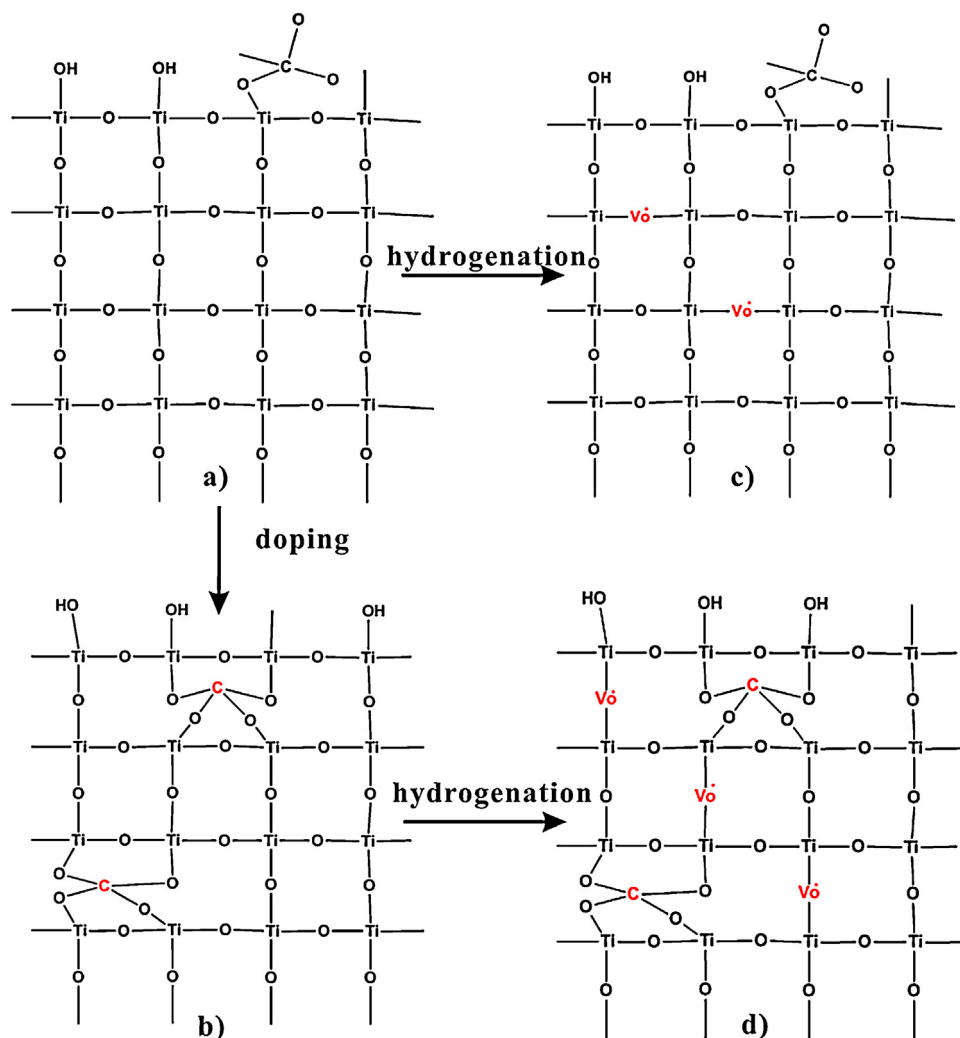
Fig. 10. Schematic illustration the microstructure evolution of (a) TiO_2, (b) C—TiO_2, (c) H—TiO_2, (d) H—C—TiO_2 after doping and hydrogenation.

decomposed into CO and H_2O, CO species finally react with active oxygen species to produce CO_2 [46]. For H—C—TiO_2, large amounts of oxygen vacancies generate while the quantity of transformed oxygen active species reduce with the amount of chemisorbed O_2 decrease, so the catalytic activity is enhanced inconspicuously.

As is well known, the semiconductor photocatalysis is initiated by the surface trapping of photo generated electrons and holes, which induces interfacial electron-transfer reactions with adsorbed organic contamination. Finally, the organic contamination is decomposed into CO_2 and H_2O. However, light illumination is not a necessary condition for our hydrogenated samples, for the fact that impurity can ionize to produce electrons in metal oxides semiconductor at room temperature.

In our work, oxygen vacancies exist and produce lots of electrons through impurity (defects) ionized, which is consistent with the literature [28]. Then the O_2 adsorbed on the surface of H—TiO_2 interact with electrons and be transformed into active oxygen species to degrade formaldehyde. If too many oxygen vacancies are introduced into the bulk of material, electrons may be trapped to prevent oxygen molecules from transforming to active oxygen species. It is considered that only the existence of an appropriate quantity concentration of oxygen vacancies could ensure that modified TiO_2 samples exhibit excellent catalytic performance. Hence, H—C—TiO_2 did not show significant improvement in the degradation of formaldehyde in the dark over H—TiO_2. The synergistic

effects between hydrogenation and C doping which are not obvious may be related to synthesis methods [47]. Thus, the relationship between the concentration of oxygen vacancies and catalytic performance is our subsequent investigation.

5. Conclusions

In this work, we have used a simple H_2 reduction strategy to obtain the H—TiO_2 catalyst with excellent catalytic activity at room temperature in the dark. The H_2 reduction strategy is much more convenient and economical than that in previous reports. However, the synergistic effects between hydrogenation and C doping are not evident. The mechanism distinguished from the traditional photocatalysis principle is tentatively proposed: the amounts of surface hydroxyl group and chemisorbed O_2 as well as the concentration of oxygen vacancy are increased after H_2 reduction. An appropriate quantity of oxygen vacancies plays an important role in decomposing formaldehyde in the dark while too many of them may suppress the catalytic activity. As a necessary component part in this process, chemisorbed O_2 and surface hydroxyl group both contribute to the excellent catalytic performance of hydrogenated TiO_2 samples. In conclusion, the catalytic activity is related to the concentration of oxygen vacancies. The relationship between the concentration of oxygen vacancies and catalytic activity needs further investigation in subsequence. This work has also presented

a promising method to improve TiO$_2$ catalyst for decomposing formaldehyde in the dark.

Acknowledgements

References

[1] A. Fujishima, K. Honda, Nature 37 (1972) 238.
[2] A. Fujishima, T.N. Rao, D.A. Tryk, J. Photochem. Photobiol. C 1 (2000) 1.
[3] D.A. Tryk, A. Fujishima, K. Honda, Electrochim. Acta 45 (2000) 2363.
[4] M. Grtäzel, Nature 414 (2001) 338.
[5] A. Hagfeldt, M. Grtäzel, Chem. Rev. 95 (1995) 49.
[6] A.L. Linsebigler, G. Lu, J.T. Yates Jr., Chem. Rev. 95 (1995) 735.
[7] A. Millis, S.L. Hunte, J. Photochem. Photobiol. A 108 (1997) 1.
[8] A. Kachina, E. Puzenat, S.O. Chikh, C. Geantet, P. Delichere, P. Afanasiev, Chem. Mater. 24 (2012) 636–642.
[9] J. Wu, Q.J. Liu, P. Gao, Z.Q. Zhu, Mater. Res. Bull. 46 (2011) 1997–2003.
[10] D.D. Camillo, F. Ruggieri, S. Santucci, L. Lozzi, J. Phys. Chem. C 116 (2012) 18427–18431.
[11] Y.Y. Wen, H.M. Ding, Y.K. Shan, Nanoscale 3 (2011) 4411.
[12] E. Barborini, A.M. Conti, I. Kholmanov, P. Piseri, A. Podestà, P. Milani, C. Cepek, O. Sakho, R. Macovez, M. Sancrotti, Adv. Mater. 17 (2005) 1842–1846.
[13] N. Lakshminarasimhan, A.D. Bokare, W.Y. Choi, J. Phys. Chem. C 116 (2012) 17531–17539.
[14] A. Zaleska, Recent Pat. Eng. 2 (2008) 157–164.
[15] Y.H. Xu, H.R. Chen, Z.X. Zeng, B. Lei, Appl. Surf. Sci. 252 (2006) 8565–8570.
[16] M.H. Zhou, J.G. Yu, J. Hazard. Mater. 152 (2008) 1229–1236.
[17] R. Akbarzadeh, S.B. Umbarkar, R.S. Sonawane, S. Takle, M.K. Dongare, Appl. Catal. A: Gen. 374 (2010) 103–109.
[18] M.C. Álvarez-Galván, B. Pawelec, V.A. Peña O'Shea, J.L.G. Fierro, P.L. Arias, Appl. Catal. B: Environ. 51 (2004) 83–91.
[19] H.B. Huang, D.Y.C. Leung, ACS Catal. 1 (2011) 348–354.
[20] J.X. Peng, S.D. Wang, Appl. Catal. B: Environ. 73 (2007) 282–291.
[21] X.B. Chen, L. Liu, P.Y. Yu, S.S. Mao, Science 331 (2011) 746.
[22] J. Zhang, Y.P. Zhang, Y.K. Lei, C.X. Pan, Catal. Sci. Technol. 1 (2011) 273–278.
[23] S. Ghosh, G.G. Khan, K. Mandal, A. Samanta, P.M.G. Nambissan, J. Phys. Chem. C 117 (2013) 8458–8467.
[24] A. Naldoni, M. Allieta, S. Santangelo, M. Marelli, F. Fabbri, S. Cappelli, C.L. Bianchi, R. Psaro, V.D. Santo, J. Am. Chem. Soc. 134 (2012) 7600–7603.
[25] W.D. Zhu, C.W. Wang, J.B. Chen, D.S. Li, F. Zhou, H.L. Zhang, Nanotechnology 12 (2012) 455204.
[26] G.M. Wang, H.Y. Wang, Y.C. Ling, Y.C. Tang, X.Y. Yang, R.C. Fitzmorris, C.C. Wang, J.Z. Zhang, Y. Li, Nano Lett. 11 (2011) 3026–3033.
[27] X.D. Jiang, Y.P. Zhang, J. Jiang, Y.S. Rong, Y.C. Wang, Y.C. Wu, C.X. Pan, J. Phys. Chem. C 116 (2012) 22619–22624.
[28] X.H. Lu, G.M. Wang, T. Zhai, M.H. Yu, J.Y. Gan, Y.X. Tong, Y. Li, Nano Lett. 12 (2012) 1690–1696.
[29] M. Fittipaldi, D. Gatteschi, P. Fornasiero, Catal. Today 206 (2013) 2–11.
[30] Y.Z. Li, D.S. Hwang, N.H. Lee, S.J. Kim, Chem. Phys. Lett. 404 (2005) 25–29.
[31] Z.Z. Zhang, J.L. Long, X.Q. Xie, H.Q. Zhuang, Y.G. Zhou, H. Lin, R.S. Yuan, W.X. Dai, Z.X. Ding, X.X. Wang, X.Z. Fu, Appl. Catal. A: Gen. 425 (2012) 117–124.
[32] B. Neumann, P. Bogdanoff, H. Tributsch, S. Sakthivel, H. Kisch, J. Phys. Chem. B 109 (2005) 16579.
[33] S. Sakthivel, H. Kisch, Angew. Chem. Int. Ed. 42 (2003) 4908.
[34] E. Papirer, R. Lacroix, J.B. Donnet, G. Nanse, P. Fioux, Carbon 33 (1995) 63.
[35] H.Q. Wang, Z.B. Wu, Y. Liu, J. Phys. Chem. C 113 (2009) 13317.
[36] R. Fu, N. Yoshizawa, M.S. Dresselhaus, G. Dresselhaus, J.H. Satcher, T.F. Baumann, Langmuir 18 (2002) 10100.
[37] J. Wu, M. Tang, Nanoscale 3 (2011) 3915–3922.
[38] H.Y. Li, D.J. Wang, H.M. Fan, P. Wang, T.F. Jiang, T.F. Xie, J. Colloid. Interf. Sci. 354 (2011) 175–180.
[39] F. Spadavecchia, S. Ardizzone, G. Cappelletti, C. Oliva, S. Cappelli, J. Nanopart. Res. 14 (2012) 1301.
[40] X.X. Zou, J.K. Liu, J. Su, F. Zuo, J.S. Chen, P.Y. Feng, Chem. Eur. J 19 (2013) 2866–2873.
[41] Z.F. Zheng, J. Teo, X. Chen, H.W. Liu, Y. Yuan, E.R. Waclawik, Z.Y. Zhong, H.Y. Zhu, Chem. Eur. J. 16 (2010) 1202–1211.
[42] C.B. Zhang, H. He, K. Tanaka, Appl. Catal. B: Environ. 65 (2006) 37–43.
[43] H.F. Li, N. Zhang, P. Chen, M.F. Luo, J.Q. Lu, Appl. Catal. B: Environ. 110 (2011) 279–285.
[44] R. Dewil, E. Kim, B. Jan, Catal. Commun. 6 (2005) 793–795.
[45] J.X. Peng, S.D. Wang, J. Phys. Chem. C 11 (2007) 9897–9904.
[46] S.S. Kim, K.H. Park, S.C. Hong, Appl. Catal. A: Gen. 398 (2011) 96–103.
[47] S. Hoang, S.P. Berglund, N.T. Hahn, A.J. Bard, C.B. Mullins, J. Am. Chem. Soc. 134 (2012) 3659–3662.